Wound healing effects of biogenic gold nanoparticles synthesized using red wine extracts

Tswellang Mgijima, Nicole R. S. Sibuyi, Adewale O. Fadaka, Samantha Meyer, Abram M. Madiehe, Mervin Meyer & Martin O. Onani

View supplementary material ⚹

Published online: 28 Jul 2024.

Submit your article to this journal ⚹

Article views: 1027

View related articles ⚹

View Crossmark data ⚹

Taylor & Francis
Taylor & Francis Group

Wound healing effects of biogenic gold nanoparticles synthesized using red wine extracts

Tswellang Mgijima[a] (ID), Nicole R. S. Sibuyi[b,c] (ID), Adewale O. Fadaka[b] (ID), Samantha Meyer[d] (ID), Abram M. Madiehe[b] (ID), Mervin Meyer[b] (ID) and Martin O. Onani[a] (ID)

ᵃOrganometallics and Nanomaterials, Department of Chemical Sciences, University of the Western Cape, Bellville, South Africa; ᵇDepartment of Science and Innovation (DSI)/Mintek Nanotechnology Innovation Centre (NIC) Biolabels Research Node, Department of Biotechnology, University of the Western Cape, Bellville, South Africa; ᶜHealth Platform, Advanced Materials Division, Mintek, Randburg, South Africa; ᵈPhytotherapy Research Group, Department of Biomedical Sciences, Cape Peninsula University of Technology, Bellville, South Africa

ABSTRACT

Gold nanoparticles (AuNPs) were synthesized using three red wine extracts (RW-Es); by varying temperature, pH, concentrations of RW-Es and gold salt. The RW-AuNPs were characterized by UV–vis, transmission electron microscopy (TEM), dynamic light scattering (DLS), and the Fourier Transform Infra-red Spectroscopy (FT–IR). Their stability was evaluated in water, foetal bovine serum (FBS), phosphate-buffered saline (PBS), and Dulbecco's Modified Eagle Medium (DMEM) by UV–Vis. The effect of the RW-Es and RW-AuNPs on KMST-6 cell cell viability was evaluated by MTT assay; and their wound healing effects were monitored by scratch assay. RW-AuNPs synthesis was observed by colour change, and confirmed by UV–Vis spectrum, with an absorption peak around 550 nm. The hydrodynamic sizes of the RW-AuNPs ranged between 10 and 100 nm. Polyphenols, carboxylic acids, and amino acids are some of functional groups in the RW-Es that were involved in the reduction of RW-AuNPs. The RW-AuNPs were stable in test solutions and showed no cytotoxicity to the KMST-6 cells up to 72 h. AuNPs synthesized from Pinotage and Cabernet Sauvignon enhanced proliferation of KMST-6 cells and showed potential as wound healing agents. Further studies are required to investigate the molecular mechanisms involved in the potential wound-healing effect of the RW-AuNPs.

Introduction

The health benefits of grapes (*Vitis vinifera*) and its products cannot be overemphasized. These fruits have been explored since time immemorial. They have been mythically and scientifically reported to reduce the risk of cardiovascular diseases and cancer [1,2]. Their sundry health attributes such as antioxidant, anticancer, anti-inflammatory, antimicrobial, anti-ulcer, hepatoprotective and cardioprotective properties, are due to their high phenolic and flavonoid contents. The widely studied wine constituents include resveratrol, chlorogenic acid, catechin and gallic acid [1]. Polyphenols were reported to play a key role as reducing, capping and stabilizing agents in the green synthesis of metal-based nanoparticles (MNPs) [3]. Evidently, grape pomace, which contains seeds, skins, and stalks, is a rich source of polyphenolic compounds, which have been reported in the synthesis of MNPs [3,4]. Although pure compounds from grape pomace have been shown to synthesize MNPs, their low solubility limits their applications. Due to the high polyphenolic content, the fermented grape

juice [3] and wine [5] were also considered for the synthesis of MNPs, including AuNPs. Wines have high alcohol content, sugars, and anthocyanins as opposed to other grape products such as the grape juice [6]. It is reported that the phenolic content in RWs is 10-fold higher than white wines. The South African trademarked Pinot noir (PN) wine has higher amount of antioxidants compared to other RWs [7]. The phenolic acids, stilbene, and flavonoids in the RWs have been widely used in medicine due to their health benefits as mentioned above [2,8], the employment of RW-Es in green synthesis is relatively unexplored. This introduces a new dimension to the biosynthesis of AuNPs that will potentially harness the distinctive bioproperties of RW-derived polyphenols. Interestingly enough, only the Georgian *Saperavi* RW has been used to synthesize AuNPs [5]. Since alcoholic beverages, including RW have been used in wound healing as aseptic agents to prevent wound infections [9], it is believed that these activities may be enhanced in their bio-synthesized AuNPs.

The global burden posed by chronic wounds on patients and the healthcare system continues to escalate and with it the mortality rates. The chronic wounds, such as diabetic foot ulcers, have a five-year mortality rate similar to that of cancer [10], yet there are not many conventional wound healing strategies in place. This growing pressure requires immediate attention and the contemporary new field of green nanotechnology may be one of the best candidates. Nanotechnology presents an innovative means of improving and modifying the existing technologies making them suitable and effective for wound healing strategies. Nanomaterials, the source matter, can be used in biomedical application as drug delivery vehicles or treatment [11,12]. Less work is available for the wound healing properties, especially where AuNPs from wine materials are applied despite the AuNPs having intrinsic properties that can aid in wound closure by enhancing cell migration. During the wound-healing process, molecular mediators such as reactive oxygen species (ROS), neutrophils, and inflammatory cytokines are released [13]. ROS is released as a by-product of cellular metabolism where the excess amounts can be detrimental to the wound healing process. The grape products and AuNPs are antioxidants that can prevent the production of the ROS thereby promoting wound healing [14], better still, a combination of the two systems might have synergistic wound healing properties further making this type of work highly attractive.

The inspiration for the green approach is motivated by the fact that it uses natural products, and researchers are always hoping to replicate nature's ability to produce small clusters of atoms that can self-assemble to produce more elaborate structures [15]. Plant extracts are of interest in green synthesis because they are readily available, inexpensive and require less energy input. The biocompatibility of gold which has resulted in its long history of application in the treatment of cancer and arthritis serves as a great advantage for its choice [16], ultimately influencing the use of AuNPs in many biomedical applications instead of other MNPs such as AgNPs, copper NPs, platinum NPs and palladium NPs. Comparatively, the AuNPs [17] and AgNPs [18] are the most widely researched MNPs owing to their medical and commercial presence, respectively. However, the major limitation for Ag-based products including AgNPs is their cytotoxicity. This reason opened a huge window for AuNPs research in various biomedical applications as drug delivery, therapeutic and diagnostic agents. All that needs to be done is for various parameters to be tuned in the control of AuNPs' cellular uptake, interaction and function [19].

Conclusively, the AuNPs are now attracting a great interest as potential wound healing agents [20] should they be incorporated into an existing ointment for a synergistic wound healing effects. In comparison to standard ointment treatment, the NP ointments healed 100% of the wounds in 19 days instead of 21 days in control animals which was a highly encouraging result [21]. Green synthesized NPs can modify conventional technologies to increase their efficiency as well as develop novel strategies that have improved properties. We believe that wine synthesis can significantly reduce the cost of development and end products [22].

Consequently, for the first time, this work reports on the synthesis of AuNPs using identified polyphenol-rich RWs. The RW-AuNPs were tested *in vitro* through scratch assay on KMST-6 cells, and their effect on cell migration was evaluated. These results are all discussed herein and hope to open a new research dimension involving one of the worldly loved products which has not been explored. Merging nanotechnology with green chemistry and biotechnology is a field like no other in addressing main sustainable development goals beyond the next decade.

Methodology

Preparation of RW-Es

The South African RWs, Van Loveren *Pinot Noir* (PN), Van Loveren African Java *Pinotage* (P), and Coral Reef *Cabernet Sauvignon* (CS) RWs, were purchased from a local liquor store (Parow Centre Mall, Cape Town, South Africa). An aliquot of 500 ml of each of the RWs was dried by a BUCHI rotary evaporator (Postfach, Switzerland) at 50 °C for 6 h [23]. The resulting paste was dried overnight in a 50 °C oven. 100 mg/ml stock solutions of the RW-Es were prepared in deionized water and stored at 4 °C until further use.

Synthesis and characterization of RW-AuNPs

The RW-AuNPs synthesis was optimized by varying the temperature (25, 30, 50, and 100 °C), RW-Es concentration (0–50 mg/ml), $HAuCl_4$ (Sigma, St Louis, USA) concentration, pH (4–10), and time, as previously described with some modifications [24,25]. Briefly, 0.04 ml of each RW-Es was added into an Eppendorf tube containing 0.36 ml of pre-warmed 1 mM $HAuCl_4$ at 1:10 ratio. The reactions were carried out on an Eppendorf Thermomixer (Hamburg, Germany) for 1 h at 1000 rpm mixing rate while observing colour changes. The necessary parameters were optimized one at a time. The formation of the RW-AuNPs was monitored by UV–Vis spectrophotometer.

Characterization of the RW-AuNPs

The RW-AuNPs were centrifuged on an Eppendorf 5417 R centrifuge (Hamburg, Germany) for 15 min at 10,000 rpm. The RW-AuNPs pellets were resuspended in a 0.4 ml of deionized water. This mixture was then diluted in a 1:10 ratio in deionized water and characterized as described in the literature [26] using; the UV–Vis recorded in a POLARstar Omega plate reader (BMG Labtech, Offenburg, Germany); by DLS to determine the hydrodynamic size, polydispersity index (PDI) and zeta potential using the Malvern Nano ZS90 Zetasizer (Malvern Panalytical Ltd. Enigma Business Park, UK). The morphology of RW-AuNPs was studied by FEI Tecnai T20 TEM (Oregon, USA), and the phytochemical groups involved in AuNPs synthesis were analyzed by FTIR PerkinElmer spectrum two™ FT–IR instrument (UK) between 4000 cm^{-1} and 400 cm^{-1} wavenumbers. The crystalline structure of the RW-AuNPs was analyzed by Bruker D8 Advance X-ray diffractometers

(Karlsruhe, Germany). The crystalline mean crystalline size (D) was calculated using the Scherrer equation (Eq. (1)).

$$D = \frac{K\lambda}{\beta\cos(\theta)} \qquad (1)$$

where $k = 1$, $\lambda = 0.1542$, β is the full width at half maximum (FWHM) and θ is the diffraction angle [27].

Effect of RW-Es and RW-AuNPs on cell viability

The KMST-6 cells were purchased from Thermofisher Scientific (Waltham, MA, USA), and a donation from Prof Denver Hendricks (Department of Clinical and Laboratory Medicine, University of Cape Town, South Africa). The cells were seeded at a cell density of 1×10^5 cells/ml^{-1} in 96-well plates (100 μl/well) and incubated for 24 h at 37 °C in a humidified 5% CO_2 incubator (Thermo electron corporation, Labotec, USA). The cells were treated with 0–1 mg/ml RW-Es and 0–50 μg/ml RW-AuNPs prepared in DMEM. Treatments with RW-AuNPs were done in quadruplicates, one of the wells was used to account for AuNPs interference. After 24 h, cell viability was assessed by the 3-(4,5-dimethylthiazol-2-yl)-2,5-diphenyltetrazolium Bromide (MTT) assay, as previously described [26]. The percentage of cell viability was calculated using Eq. (2):

$$\% \text{ Cell viability} = \left(\frac{untreated}{treated}\right) \times 100\% \qquad (2)$$

Effect of RW-Es and RW-AuNPs on wound healing

The *in vitro* scratch assay was performed on KMST-6 cells to evaluate the effect of treatments on cell migration following a reported protocol [28]. Briefly, 2×10^5 cells/ml were seeded onto a 24-well sterile plate and incubated for 24 h at 37 °C. A scratch was created by a sterile 200 μl pipette tip across the centre. The detached cells were washed off with PBS and treated with 0.25 mg/ml of RW-Es, 50 μg/ml RW (PN, CS, P)-AuNPs and 50 μg/ml Allantoin prepared in DMEM supplemented with 1% FBS. The wound gap was viewed under EVOS XL core light microscope (Invitrogen, USA) and images were taken at 0–72 h at 10× magnification. The images were analyzed using ImageJ (https://imagej.nih.gov/ij/download.html). The % wound closure was calculated using Eq. (3):

$$\% \text{Wound closure} = \frac{(pre-migration)-(migration)}{pre-migration} \times 100\% \qquad (3)$$

'Pre-migration' is the initial area of the wound at 0 h and 'migration' is the wound area after a particular time point (24–72 h). After 72 h, the total cell count was performed using Trypan blue dye exclusion assay using a haemocytometer.

Statistical analysis

The data are presented as mean ± standard deviation, which were obtained from three independent experiments that were performed in triplicates. The difference between the means was considered to be significant when $p < .05$ according to two-way ANOVA.

Results and discussion

The bio-inspired synthesis of AuNPs is becoming popular with increasing environmental impact consciousness. Not only are these methods eco-friendly, but also cost-effective and a rapid form of MNP synthesis. The AuNPs are of particular interest as they are the most stable form of MNPs [29] and have been synthesized from numerous plant extracts, for examples *Dracocephalum kotschi* [30] and *Elaise guineensis* [29]. The extracts may be from the peels, fruits, stems, and roots [31]. It is known that the plants contain metabolites such as polyphenols, sugars, proteins, terpenoids and alkaloids which play a role in the reduction of gold salt to their metallic AuNPs and ensure their stability [32]. Synthesis occurs in a single step, and the mechanism of the biosynthesis of NPs from plants is based on the cellular uptake mechanisms, combination of phytochemicals, enzymes and biomolecules they possess. Generally, due to mentioned properties, plants have been used in the extraction of metals from biomass to return an economic profit [33]. In the current study, RW-Es were explored for the synthesis of AuNPs.

Biosynthesis of RW-AuNPs

The RW-AuNPs were produced through green synthesis as depicted in the reaction scheme shown in Figure S1. Different reaction parameters have a significant impact on the physico-chemical properties of AuNPs, such as their shape, size, and surface charge [34]. The reaction conditions that favour green synthesis and formation of stable RW-AuNPs [22, 35], such as temperature, pH, incubation time, concentrations of RW-Es and $HAuCl_4$ were optimized. One or two parameters were varied at a time while the others were kept constant, and the progress of the reaction was monitored visually and by UV–Vis spectra. The colour change to brick-red or wine-red was a first indication of the formation of RW-AuNPs [36], and this was further confirmed by the uniformed SPR peak at ~500 nm using the UV–Vis [37].

The SPR provides information about the size, morphology, and relative concentration of the AuNPs. The SPR is an important phenomenon influenced by the inter-particle distance, electron density, and the refractive index of the reaction medium [38]. These factors can be tuned by altering the reaction parameters, most of which are investigated in this study. A change in absorbance to a longer wavelength (the red-shift) result from an increase in particle size and a reduction in particle size gives a shorter wavelength or blue shift [39].

The optimal conditions for the biosynthesis of RW-AuNPs are described in detail in the supplementary materials (Figures S2–S4) and summarized in Table 1. PN-AuNPs were synthesized using 25 mg/ml of PN-E at pH 6 at 25 °C; CS-AuNPs were synthesized with 12.5 mg/ml of CS-E at pH 4 at 50 °C; and P-AuNPs were synthesized with 50 mg/ml of P-E at pH 5 at

Table 1. Optimal conditions for RW-AuNPs synthesis.

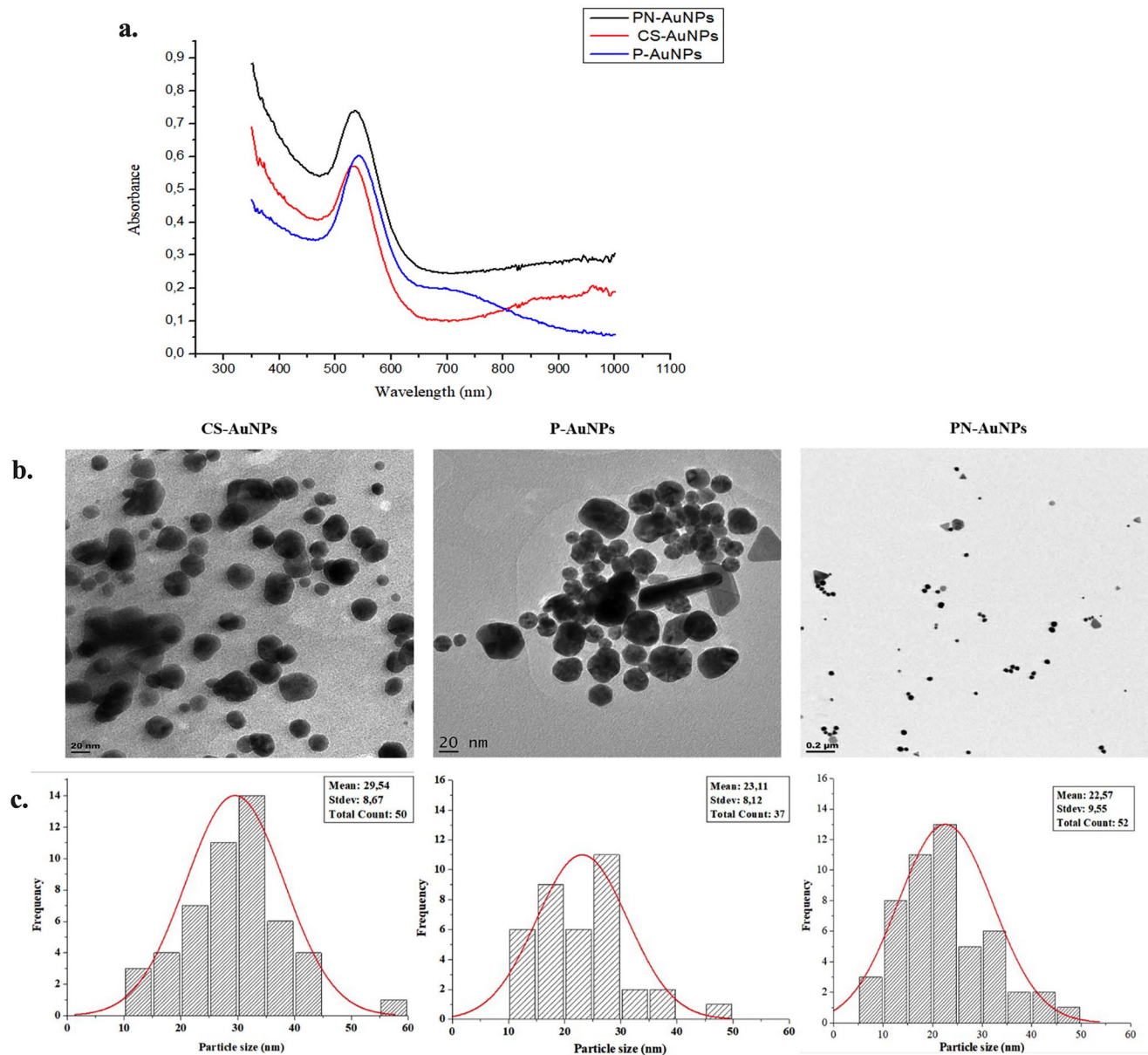| RW-Es	RW-Es stock (mg/ml)	$HAuCl_4$ (mM)	RW-Es: Au salt	Temperature (°C)	pH	Reaction time (h)
PN-E	25	1	1:10	25	6	2.5
P-E	50	1	1:10	50	5	2
CS-E	12.5	1	1:5	50	4	2

Figure 1. UV–vis (a), HR-TEM micrographs (b) and histogram for size distribution (c) of RW-AuNPs.

50 °C. PN- and P-AuNPs were synthesized using 1 mM $HAuCl_4$ using a 1:10 ratio, and 1:5 for CS-AuNPs. These parameters do vary from plant to plant and may be optimized by simply varying the reaction parameters. However, while it is desirable to synthesize AuNPs at ambient temperatures, studies show that not all plant extracts can readily generate the nanoparticles at temperatures below 25 °C [24].

The spectra for the RW-AuNPs were symmetrical with SPR peaks at 542, 544, and 540 nm for P-AuNPs, PN-AuNPs and CS-AuNPs, respectively (Figure 1(a)). The P-AuNPs had two absorption peaks, at 540 and 710 nm, corresponding to the transverse and longitudinal plasmon modes. The two peaks suggested a presence of non-spherical AuNPs [40]. Quantitatively, the nanospheres were more than other shapes since the transverse peak was dominant [41]. This was confirmed by the HRTEM micrograms, showing spherical and triangular-shaped RW-AuNPs (Figure 1(b)). The anisotropic shapes are common in biogenic NPs, and this is associated with various phytochemicals present in the extracts, as reported for AuNPs synthesized by various plant extracts [24], such as *Terminalia mantaly* [42] and *Cyclopia intermedia* [26]. The RW-AuNPs had core size distribution in the range 10 – 60 nm, the average core sizes for the CS-, P- and PN-AuNPs were 29.54, 23.11 and 22.57 nm, respectively.

DLS analysis

The CS-AuNPs had the lowest hydrodynamic size (48.76 nm) compared to P-AuNPs (85.87 nm) and PN-AuNPs (82.13 nm) (Table 2). The hydrodynamic size accounts for the core size as well as the surface composition [37, 42]. The PDI of the RW-AuNPs ranged between 0.2 and 0.5, affirming that the RW-Es produced monodispersed and stable RW-AuNPs. CS-AuNPs had the lowest PDI of 0.205. Although PN-AuNPs and P-AuNPs had a relatively large PDI of 0.386 and 0.444, respectively, they were still considered to be monodispersed considering that these PDI values were all below 0.5. The PDI ranges between 0 and 1, where the poly-dispersed particles have higher PDI, typically ≥0.7, and the PDI for monodispersed particles is below 0.5 [43]. The zeta potential of the RW-AuNPs was greater than + 40 mV, which is +10 mV above the stability index of +30 mV [44].

XRD analysis

The crystalline structure of the RW-NPs was determined by XRD analyzed in the range of 2θ between 20° and 85°. Diffraction peaks appeared around 38°, 44°, 64° and 77° for the RW-AuNPs as shown in Figure 2. These peaks are related to the prominent peaks (1 1 1), (2 0 0), (2 2 0) and (3 1 1) Bragg reflection planes of a face-centered cubic structure of gold [45]. These peaks confirmed the crystalline nature of the RW-AuNPs. The unassigned peaks could be related to the production of bio-organic crystalline on the surface of the RW-AuNPs [27].

The average crystalline size was calculated to be 8.89, 9.22 and 9.21 nm for P-, PN- and CS-AuNPs, respectively, as shown in Table 3.

Table 2. Optical and DLS properties of RW-AuNPs.

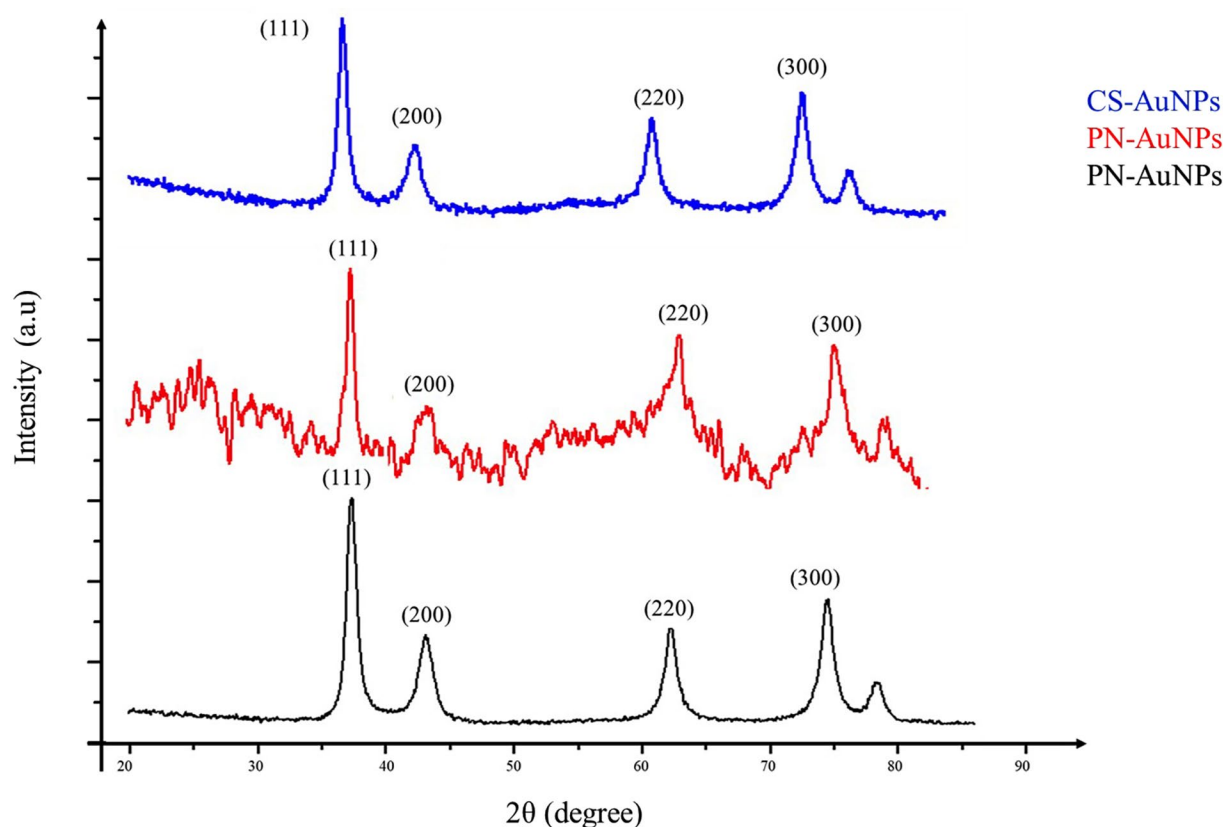| AuNPs	RW-Es (mg/ml)	SPR (nm)	Hydrodynamic size (d.nm)	Zeta potential (mV)	PDI
PN-AuNPs	25	544	82.13	+51.60±2.2	0.386±0.04
CS-AuNPs	12.5	540	48.76	+41.69±3.69	0.205±0.05
P-AuNPs	50	542	85.87	+50.76±1.74	0.444±0.03

Figure 2. XRD spectrum of RW-AuNPs.

Table 3. Crystalline sizes calculation of RW-AuNPs using the Scherrer equation.

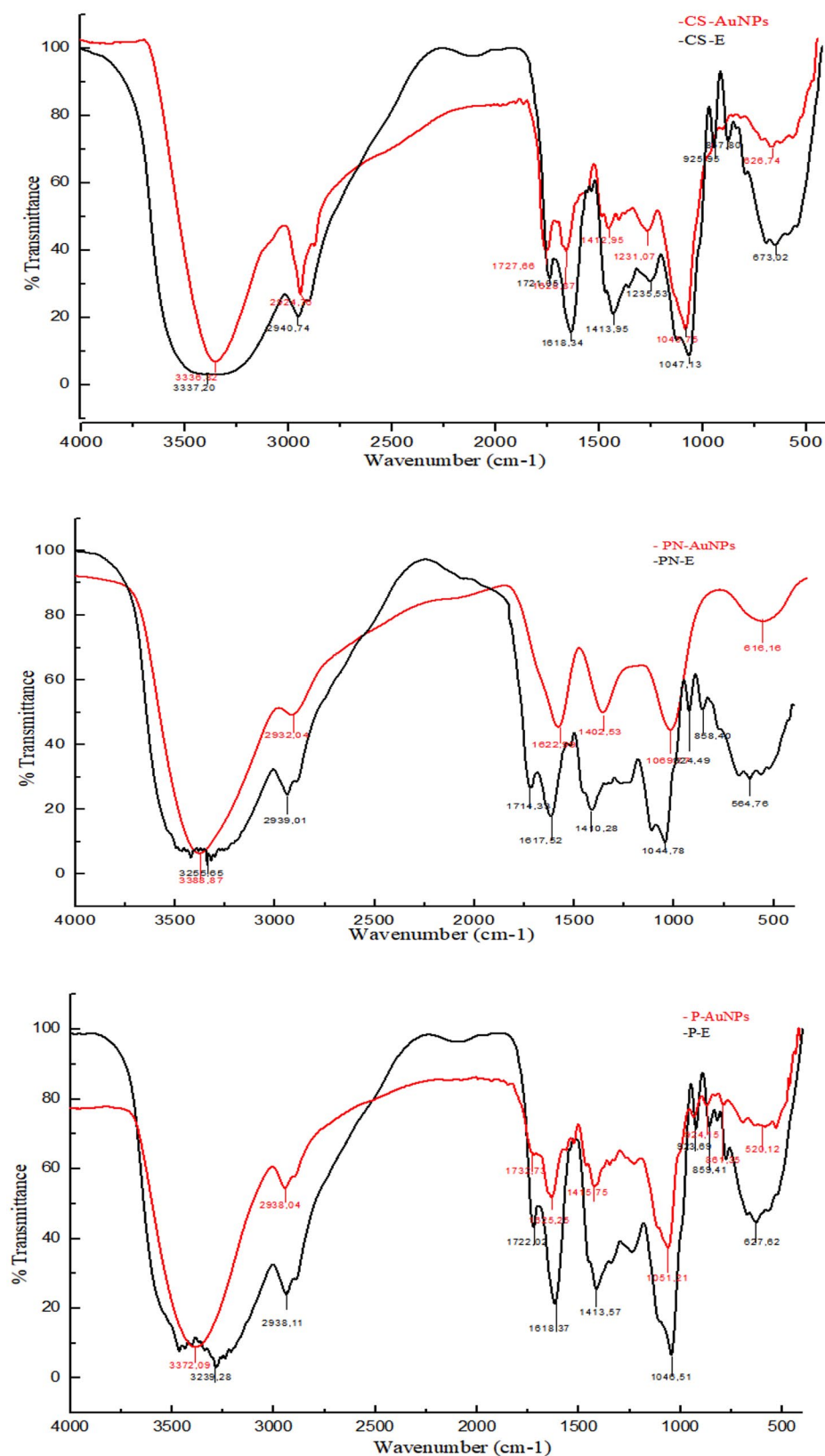| Bragg reflection planes	P-AuNPs			PN-AuNPs			CS-AuNPs		
	Peak position (2θ)	FWHM	Diameter (nm)	Peak position (2θ)	FWHM	Diameter (nm)	Peak position (2θ)	FWHM	Diameter (nm)
111	38.5	0.9	10.0	38.2	0.6	15.3	38.3	0.9	10.7
200	44.6	1.3	7.3	44.4	1.7	5.5	44.4	1.3	7.5
220	64.9	1.1	9.1	64.6	2.1	4.9	64.8	1.2	9.0
311	77.8	1.3	9.1	77.6	1.0	11.2	77.8	1.2	9.6
Average			8.9			9.2			9.2

Figure 3. FT–IR spectra of RW-Es and the RW-AuNPs.

FT–IR analysis

The FT–IR spectra of RW-Es and RW-AuNPs demonstrated that phytochemicals in RW-Es played a role in the reduction of Au^+ to Au^0. As shown in Figure 3, there were noticeable

similarities between RW-Es and RW-AuNPs spectra. Some of the peaks were transmitted at the same wavelengths suggesting that some phytochemicals present in the RW-Es were also present on the surface of the RW-AuNPs. The bands that were shifted in RW-AuNPs as compared to the RW-Es, are

summarized in Table S1. RWs are rich in polyphenolic compounds such as tannins, anthocyanins, catechins and flavonoids [8], and the transmittance of O–H and C–O at 1680 and 900 cm^{-1}, validated their involvement in the RW-AuNPs synthesis. In particular, the 1285 cm^{-1}, reported as characteristic of flavonoid-based tannins [46,47]. There was a significant reduction in the broad O–H peak between 3000 and 4000 cm^{-1} for the RW-Es compared to the RW-AuNPs [30]. The C=O group identified between 1600 and 1400 cm^{-1} indicated the presence of carboxylic acids and was more defined in the RW-Es. The polyphenols in RW-Es, evident in broad and smaller OH peak, proved that the carboxylic polyphenols were responsible for reducing Au$^+$ to Au^0. The hydroxyl-containing compounds has been reported as reducing, stabilising, and capping agents in the synthesis of AuNPs [48]. The bands around 700 to 900 cm^{-1} and 950 to 1285 cm^{-1}, were attributed to the aromatic C-H out-of-plane and in-plane, respectively [49]. The significant shifts around 1400 cm^{-1} suggested the involvement of esters, carboxylic acids [30], amino acids [50] and aromatic esters in the bio-reduction of the RW-AuNPs as reducing and stabilising agents [51].

Wound healing effects of RW-AuNPs

Phytomedicine has shaped the history of medicine, and resulted in discovery of cancer drugs (paclitaxel) and analgesics (morphine) [52]. Plant-derived drugs still continue to lead in the discovery and development of novel and improved treatments [52] for various diseases, including wound healing. A number of plant products, such as herbs, teas, fruits, etc., are reported to possess wound healing properties [53], and have been incorporated in various wound healing agents over the years [54]. Grape products were among the herbal therapies with long history in wound healing therapy [55], their bioactivities were attributed to a number of phytochemicals, especially resveratrol [56]. RW, in particular, was used as an antiseptic to prevent bacterial infections, and later used as a wound healing agent [9].

Effect of RW-Es and RW-AuNPs on KMST-6 cells

AuNPs have great potential in biomedical applications such as drug delivery, imaging, diagnostic, and therapeutic agents [17]. However, there is limited information about their impact on human health when used in short- and long- term applications. Unlike their bulk counterparts, AuNPs possess unique physicochemical properties which allow them to penetrate and accumulate in the cells [57], and therefore, their toxicity on cells ought to be evaluated before clinical applications. The effect of RW-Es and RW-AuNPs on skin fibroblast (KMST-6) cells was assessed by MTT assay, which is based on the mitochondrial activity of viable cells to reduce the yellow tetrazolium salt into a purple formazan. The colour intensity is directly proportional to the number of viable cells [58].

The CS-E, P-E and their respective AuNPs were non-toxic to the cells after 24 h treatment at all tested concentrations, as shown in Figure 4. Their effect on cell viability was dose-dependent and showed a noticeable increase in cell viability as their concentration increased. P-E (Figure 4(a)) and P-AuNPs (Figure 4(b)) had the highest effect compared to CS-E and CS-AuNPs. At 50 µg/ml, the cells reached viability of ~119% for the CS-AuNPs, and 132% for P-AuNPs, after 24 h. The PN-E and PN-AuNPs reduced the cell viability in a concentration-dependent manner. There was no significant toxicity to the cells treated with P-AuNPs and CS-AuNPs, which suggested the potential biocompatibility of these AuNPs in biological applications.

Effects of RW-AuNPs on cell migration

The possibility of the RW-AuNPs to promote *in vitro* wound closure was investigated further by a scratch assay [11], which has been successfully and extensively used to investigate the effects of various compounds, extracts and NPs on cell migration [59]. Figure 5 illustrates the change in wound gap over 72 h of treatment with RW-Es and RW-AuNPs. The images show a time-dependent closure of the scratch. Although the RW-Es treatments were used at a concentration (0.25 mg/ml) that was five times higher compared to RW-AuNPs (50 µg/ml), they failed to completely close the scratch in 72 h. The effects of RW-AuNPs were comparable to other plant extract-derived AuNPs that were reported to promote wound healing that was attributed to the extracts such as *Plectranthus aliciae* ethanolic extract [60]. The wound closure for P-AuNPs and CS-AuNPs treated cells was faster than that of the cells treated with RW-Es. The overall wound closure for the CS-AuNPs and P-AuNPs was faster than that of the untreated cells (negative control). The cells treated with Allantoin as a positive control, CS-AuNPs, and P-AuNPs appeared to have overgrown after 72 h when compared to the untreated cells. After 48 h of treatment, the wound closure for P-AuNPs and allantoin had already reached 80% closure. The wound gap on cells exposed to PN-E and their corresponding AuNPs did not completely close after 72 h. P-AuNPs followed by CS-AuNPs had comparable effects to those of allantoin, indicating their potential wound healing effects.

The rate of the wound closure for each treatment is shown in Figure 6. There was a linear relationship between gap closure rate and gap area, and the 2D continuum model of collective cell migration [61] had predicted this behaviour. All wounds treated with RW-Es did not close within the 72 h including PN-AuNPs with a wound closure of less than 50%. All treatments had the highest wound closure rate within the first 48 h except for the non-efficacious PN-AuNPs. P-AuNPs had the highest wound closure rate for the first 48 h with ~62% of the wound closing in the first 24 h. The wound healing significantly slowed down for all RW-Es, P-AuNPs and allantoin in the last 24 h of treatment; however, the closure rate was maintained for the untreated and the CS-AuNPs. The comparative activities of P-AuNPs and CS-AuNPs with allantoin, a well-known wound healing agent, positions these NPs as potential alternatives or adjuncts in wound healing therapies. This comparison is crucial for contextualising the efficacy of RW-AuNPs within the landscape of existing treatments and underscores their potential clinical relevance. These findings highlight the innovative nature of this study and position RW-AuNPs as valuable
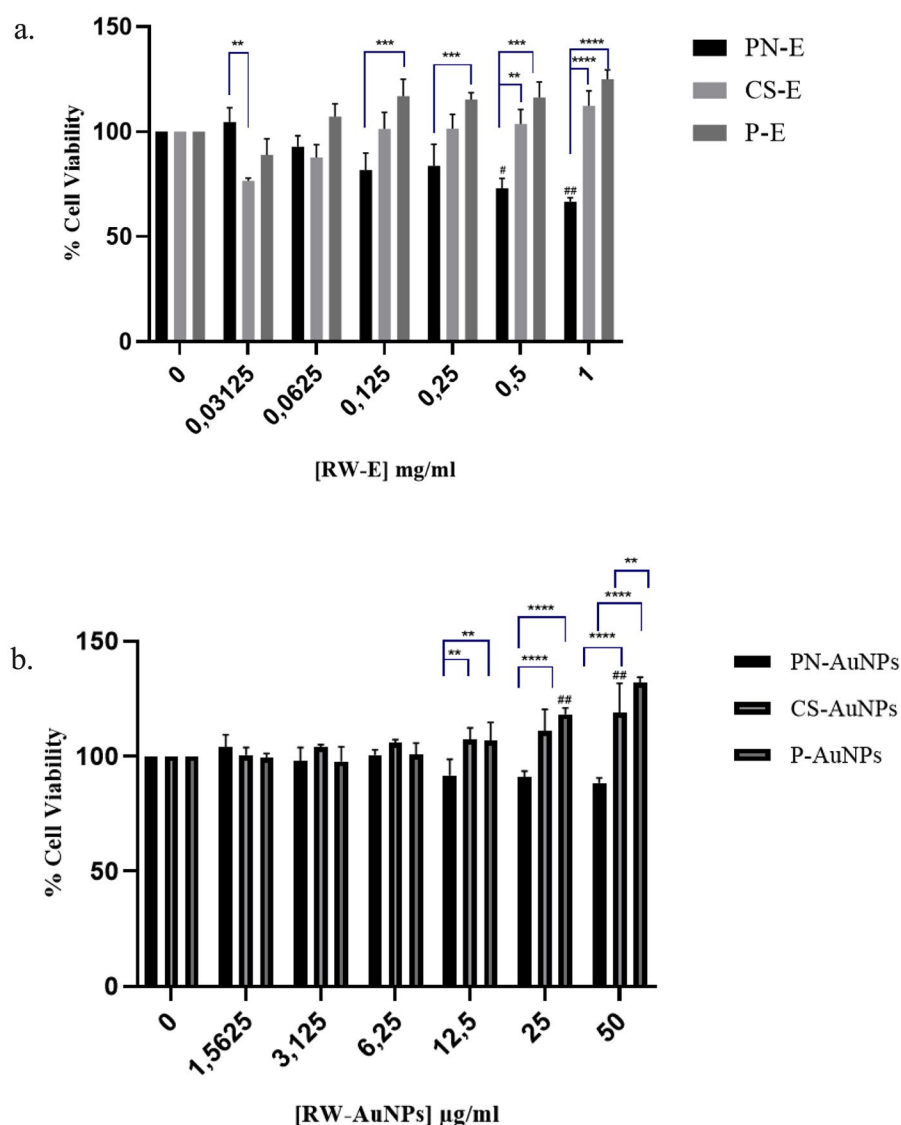
Figure 4. Effect of RW-Es and RW-AuNPs on KMST-6 cells. The cells were treated with increasing concentrations of RW-Es (a) and RW-AuNPs (b) for 24 h. Differences are considered statistically significant at $p < .05$, represented by # and * when compared to untreated and other treatments, respectively.

candidates for further biomedical research and potential clinical applications. The *in vitro* efficacy of RW-AuNPs could be translated into clinical applications, and be explored in development of wound healing regimens.

As shown in Table 4, PN-AuNPs followed by RW-Es had the lowest number of viable cells after the 72 h of treatment. The number of viable cells after 72 h was higher for allantoin (180%) followed by P-AuNPs (110%) and CS-AuNPs (92%). Allantoin is a well-known cell growth enhancer [28,62], which promoted HaCaT cell proliferation at ≤10 μg/ml [28]. In the current study, allantoin at the similar concentration (50 μg/ml) of the RW-AuNPs, had the highest number of viable cells followed by P-AuNPs and CS-AuNPs. The CS-AuNPs and P-AuNPs can be considered as the growth enhancers, while PN-AuNPs appeared to have suppressed cell growth. The increase in cell density may also be due to proliferation of the cells within the wells and not cell migration towards the scratch for the RW-Es and RW-AuNPs.

Plant extract-synthesized AuNPs have shown potential in wound healing as antibacterial, growth enhancer, and

antioxidant agents [63]. *Galenia africana* and *Hypoxis hemerocallidea* AuNPs exhibited antibacterial activity against Gram-positive and Gram-negative bacteria [24], a critical property for chronic wound healing. AuNPs were also shown to possess anti-inflammatory and immune modulatory properties [64], and promoted angiogenesis [65]; suggesting that AuNPs could have multiple effects in the wound healing process.

Conclusion

This study showed that RW-Es served as both the reducing and stabilising agents for synthesis of RW-AuNPs. A colour change from yellow to a wine-red indicated the presence of RW-AuNPs and was further confirmed by a SPR between 540 to 560 nm, which is a characteristic of AuNPs. Altering the reaction parameters such as temperature, pH and concentrations tuned the size and shape of the RW-AuNPs. Various functional groups in the RW-AuNPs were identified by FT-IR, and suggested that the
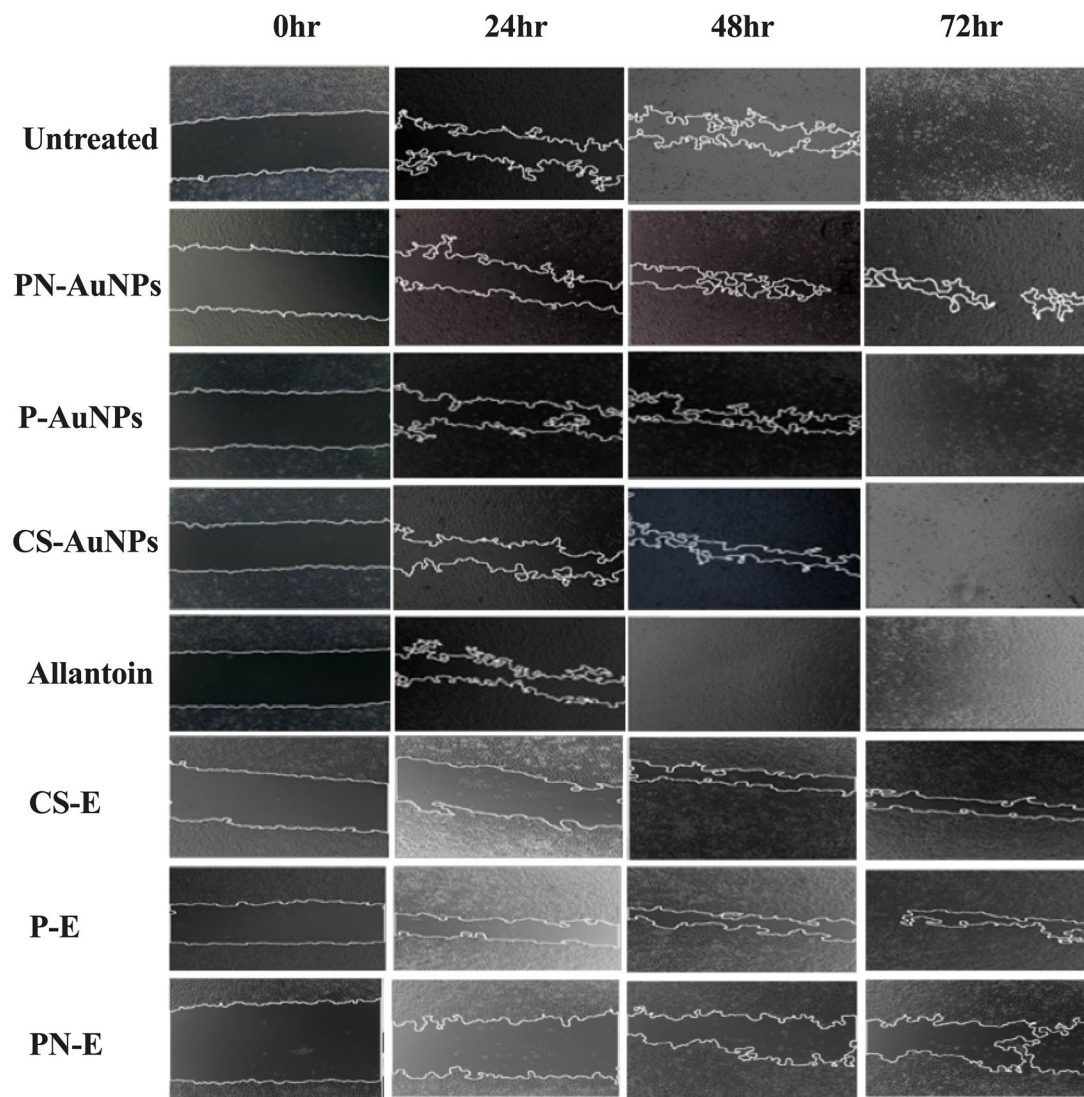
Figure 5. Effect of RW-AuNPs, RW-Es and allantoin on KMST-6 cell migration using a scratch assay. Wound gaps were assessed at 0 to 72 h after treatment with RW-AuNPs and RW-Es. Untreated: negative control; allantoin: positive control.
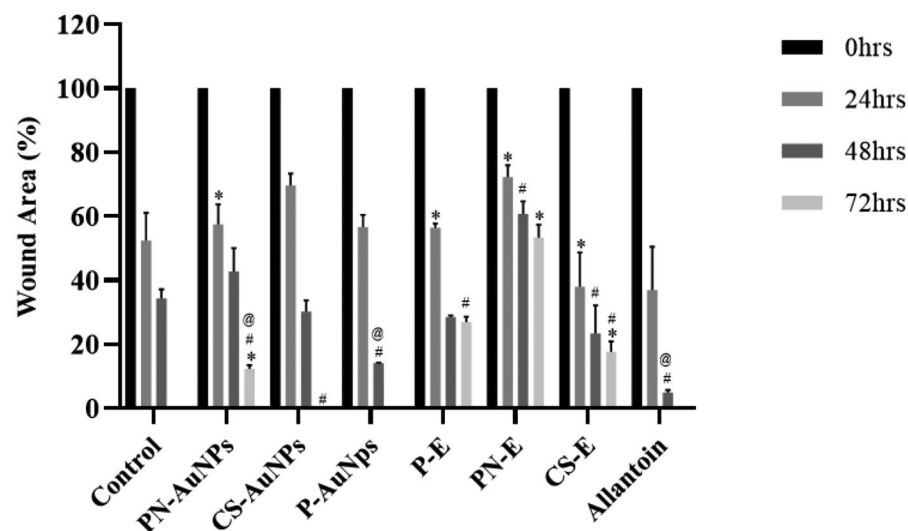

Figure 6. Wound area (%) on KMST-6 cells after treatment with RW-Es, RW-AuNPs and allantoin compared to untreated cells. Differences considered statistically significant at $p < .05$, represented by *, # and @ when compared to untreated, PN-E and CS-E respectively.

Table 4. Cell density before and 72 h after treatments.

Treatment	0 h (cells/ml)	72 h (cells/ml)	Increase in cell number (%)
Untreated	2×10^5	3.72×10^5	86
CS-E	2×10^5	2.60×10^5	30
PN-E	2×10^5	2.45×10^5	22
P-E	2×10^5	2.68×10^5	34
CS-AuNPs	2×10^5	3.84×10^5	92
PN-AuNPs	2×10^5	2.36×10^5	18
P-AuNPs	2×10^5	4.2×10^5	110
Allantoin	2×10^5	5.6×10^5	180

polyphenols, amino acids and esters were most likely to be involved in the reduction of Au^+. The CS-AuNPs and P-AuNPs were not cytotoxic to KMST-6 cells, and accelerated wound closure by enhancing cell growth. These results suggested that RW-AuNPs could be considered as wound healing and growth enhancing agents, and therefore could be incorporated into wound healing regimens. More studies are needed to confirm this activity in other cell types (skin cells and fibroblasts), their specificity and mechanisms of action *in vivo*, to validate their wound-healing properties.

Acknowledgements

Ethics approval and consent to participate

Not applicable

Consent for publication

All authors read the manuscript and consent to its publication in this journal.

Author contributions

MOO, MM and AMM conceptualized, designed methods, provided resources and obtained funding for the study. TM, NRSS, AOF and SM performed the experiments and analyzed the data. TM wrote the first draft. All the authors reviewed and edited the manuscript.

Disclosure statement

No potential conflict of interest was reported by the author(s).

Availability of data and material

The data in this is available from authors upon reasonable request.

Funding

ORCID

Tswellang Mgijima http://orcid.org/0000-0002-2002-4574
Nicole R. S. Sibuyi http://orcid.org/0000-0001-7175-5388
Adewale O. Fadaka http://orcid.org/0000-0002-3952-2098
Samantha Meyer http://orcid.org/0000-0002-5167-0608
Abram M. Madiehe http://orcid.org/0000-0002-3935-467X
Mervin Meyer http://orcid.org/0000-0002-8296-4860
Martin O. Onani http://orcid.org/0000-0002-4735-3669

References

[1] Yang J, Xiao YY. Grape phytochemicals and associated health benefits. Crit Rev Food Sci Nutr. 2013;53(11):1202–1225. doi: 10.1080/10408398.2012.692408.

[2] Xiang L, Xiao L, Wang Y, et al. Health benefits of wine: don't expect resveratrol too much. Food Chem. 2014;156:258–263. doi: 10.1016/j.foodchem.2014.01.006.

[3] Dzimitrowicz A, Jamroz P, DiCenzo GC, et al. Fermented juices as reducing and capping agents for the biosynthesis of size-defined spherical gold nanoparticles. J Saudi Chem Soc. 2018;22(7):767–776. doi: 10.1016/j.jscs.2017.12.008.

[4] Amarnath K, Mathew NL, Nellore J, et al. Facile synthesis of biocompatible gold nanoparticles from Vites vinefera and its cellular internalization against HBL-100 cells. Cancer Nanotechnol. 2011;2(1-6):121–132. doi: 10.1007/s12645-011-0022-8.

[5] Pavliashvili T, Kalabegishvili T, Janjalia M, et al. Synthesis of gold nanoparticles from chloroauric acid using the red wine. ECB. 2017;6(5):192. doi: 10.17628/ecb.2017.6.192-195.

[6] Cosme F, Pinto T, Vilela A. Phenolic compounds and antioxidant activity in grape juices: a chemical and sensory view. Beverages. 2018;4(1):22. doi: 10.3390/beverages4010022.

[7] Elangkovan DRAJ, Ganapathy D. Benefits of red wine - a review. J Contemp Issues Bus Gov. 2021;26 (2):1982–1989.

[8] Snopek L, Mlcek J, Sochorova L, et al. Contribution of red wine consumption to human health protection. Molecules. 2018;23(7):1684. doi: 10.3390/molecules23071684.

[9] Daglia M, Papetti A, Grisoli P, et al. Antibacterial activity of red and white wine against oral streptococci. J Agric Food Chem. 2007;55(13):5038–5042. doi: 10.1021/jf070352q.

[10] Sen CK. Human wound and its burden: updated 2020 compendium of estimates. Adv Wound Care (New Rochelle). 2021;10(5):281–292. doi: 10.1089/wound.2021.0026.

[11] Naskar A, Kim KS. Recent advances in nanomaterial-based wound-healing therapeutics. Pharmaceutics. 2020;12(6):499. doi: 10.3390/pharmaceutics12060499.

[12] Mordorski B, Rosen J, Friedman A. Nanotechnology as an innovative approach for accelerating wound healing in diabetes. Diabetes Manag. 2015;5(5):329–332. doi: 10.2217/dmt.15.28.

[13] Eming SA, Krieg T, Davidson JM. Inflammation in wound repair: molecular and cellular mechanisms. J Invest Dermatol. 2007;127(3):514–525. doi: 10.1038/sj.jid.5700701.

[14] Mihai MM, Dima MB, Dima B, et al. Nanomaterials for wound healing and infection control. Materials (Basel). 2019;12(13):1. doi: 10.3390/ma12132176.

[15] Saleh HEM, Koller M. Introductory chapter: principles of green chemistry. In Green Chemistry. InTechOpen Limited: London, UK; 2018.

[16] Wang S, Lu G. Applications of gold nanoparticles in cancer imaging and treatment. In Noble and Precious Metals - Properties Nanoscale Effects and Application. InTechOpen Limited: London, UK; 2018. Vol. 1, p. 291–309.

[17] Sibuyi NRS, Moabelo KL, Fadaka AO, et al. Multifunctional gold nanoparticles for improved diagnostic and therapeutic applications: a review. Nanoscale Res Lett. 2021;16(1):174. doi: 10.1186/s11671-021-03632-w.

[18] Simon S, Sibuyi NRS, Fadaka AO, et al. Biomedical applications of plant extract-synthesized silver nanoparticles. Biomedicines. 2022;10(11):2792. doi: 10.3390/biomedicines10112792.

[19] Báez DF, Gallardo-Toledo E, Oyarzún MP, et al. The influence of size and chemical composition of silver and gold nanoparticles on in vivo toxicity with potential applications to central nervous system diseases. Int J Nanomedicine. 2021;16:2187–2201. doi: 10.2147/IJN.S260375.

[20] Niska K, Zielinska E, Radomski MW, et al. Metal nanoparticles in dermatology and cosmetology: interactions with human skin cells. Chem Biol Interact. 2018;295:38–51. doi: 10.1016/j.cbi.2017.06.018.

[21] Shanmugasundaram T, Radhakrishnan M, Gopikrishnan V, et al. In vitro antimicrobial and in vivo wound healing effect of actinobacterially synthesised nanoparticles of silver, gold and their alloy. RSC Adv. 2017;7(81):51729–51743. doi: 10.1039/C7RA08483H.

[22] Eskandari-Nojehdehi M, Jafarizadeh-Malmiri H, Rahbar-Shahrouzi J. Optimization of processing parameters in green synthesis of gold nanoparticles using microwave and edible mushroom (Agaricus bisporus) extract and evaluation of their antibacterial activity. Nanotechnol Rev. 2016;5:537.

[23] Chalons P, Courtaut F, Limagne E, et al. Red wine extract disrupts Th17 lymphocyte differentiation in a colorectal cancer context. Mol Nutr Food Res. 2020;64(11):e1901286.

[24] Elbagory AM, Cupido CN, Meyer M, et al. Large scale screening of southern African plant extracts for the green synthesis of gold nanoparticles using microtitre-plate method. Molecules. 2016;21(11):1498. doi: 10.3390/molecules21111498.

[25] Dube P, Meyer S, Madiehe A, et al. Antibacterial activity of biogenic silver and gold nanoparticles synthesized from Salvia africana-lutea and Sutherlandia frutescens. Nanotechnology. 2020;31(50):505607. doi: 10.1088/1361-6528/abb6a8.

[26] Aboyewa JA, Sibuyi NRS, Meyer M, et al. Gold nanoparticles synthesized using extracts of cyclopia intermedia, commonly known as honeybush, amplify the cytotoxic effects of doxorubicin. Nanomaterials. 2021;11(1):132. doi: 10.3390/nano11010132.

[27] Hutchinson N, Wu Y, Wang Y, et al. Green synthesis of gold nanoparticles using upland cress and their biochemical characterization and assessment. Nanomaterials. 2021;12(1):28. doi: 10.3390/nano12010028.

[28] Kim J, Shin YK, Kim KY. Promotion of keratinocyte proliferation by Tracheloside through ERK1/2 stimulation. Evid Based Compl Altern Med. 2018;2018:1–5. doi: 10.1155/2018/4580627.

[29] Ahmed, Shakeel, Ikram, Saiqa, Yudha S, Salprima, Annu, Biosynthesis of gold nanoparticles : a green approach, J Photochem Photobiol B. 161, 141, 153(2016). doi: 10.1016/j.jphotobiol.2016.04.034.

[30] Dorosti N, Jamshidi F. Plant-mediated gold nanoparticles by Dracocephalum kotschyi as anticholinesterase agent: synthesis, characterization, and evaluation of anticancer and antibacterial activity. J Appl Biomed. 2016;14(3):235–245. doi: 10.1016/j.jab.2016.03.001.

[31] Kuppusamy P, Yusoff MM, Maniam GP, et al. Biosynthesis of metallic nanoparticles using plant derivatives and their new avenues in pharmacological applications – an updated report. Saudi Pharm J. 2016;24(4):473–484. doi: 10.1016/j.jsps.2014.11.013.

[32] Marslin G, Siram K, Maqbool Q, et al. Secondary metabolites in the green synthesis of metallic nanoparticles. Materials (Basel). 2018;11(6):940. doi: 10.3390/ma11060940.

[33] Sheoran V, Sheoran AS, Poonia P. Phytomining: a review. Miner Eng. 2009;22(12):1007–1019. doi: 10.1016/j.mineng.2009.04.001.

[34] Lee SH, Jun BH. Silver nanoparticles: synthesis and application for nanomedicine. Int J Mol Sci. (Basel). 2019;20(4). doi: 10.3390/ijms20040865.

[35] El Domany EB, Essam TM, Ahmed AE, et al. Biosynthesis physico-chemical optimization of gold nanoparticles as anti-cancer and synergetic antimicrobial activity using Pleurotus ostreatus fungus. J Appl Pharm Sci. 2018;8:119.

[36] Alberti G, Zanoni C, Magnaghi LR, et al. Gold and silver nanoparticle-based colorimetric sensors: new trends and applications. Chemosensors. 2021;9(11):305. doi: 10.3390/chemosensors9110305.

[37] Sibuyi NRS, Thipe VC, Panjtan-Amiri K, et al. Green synthesis of gold nanoparticles using Acai Berry and Elderberry extracts and investigation of their effect on prostate and pancreatic cancer cells. BJGP Open. 2021;8:1.

[38] Rauh A, Honold T, Karg M. Seeded precipitation polymerization for the synthesis of gold-hydrogel core-shell particles: the role of surface functionalization and seed concentration. Colloid Polym Sci. 2016;294(1):37–47. doi: 10.1007/s00396-015-3782-6.

[39] Brause R, Möltgen H, Kleinermanns K. Characterization of laser-ablated and chemically reduced silver colloids in aqueous solution by UV/VIS spectroscopy and STM/SEM microscopy. Appl Phys B Lasers Opt. 2002;75(6-7):711–716. doi: 10.1007/s00340-002-1024-3.

[40] Philip D. Synthesis and spectroscopic characterization of gold nanoparticles. Spectrochim Acta A Mol Biomol Spectrosc. 2008;71(1):80–85. doi: 10.1016/j.saa.2007.11.012.

[41] Shi W, Casas J, Venkataramasubramani M, et al. Synthesis and characterization of gold nanoparticles with plasmon absorbance wavelength tunable from visible to near infrared region. ISRN Nanomater. 2012;2012:1–9. doi: 10.5402/2012/659043.

[42] Majoumouo MS, Sharma JR, Sibuyi NRS, et al. Synthesis of biogenic gold nanoparticles from terminalia mantaly extracts and the evaluation of their in vitro cytotoxic effects in cancer cells. Molecules. 2020;25(19):4469. doi: 10.3390/molecules25194469.

[43] Danaei M, Dehghankhold M, Ataei S, et al. Impact of particle size and polydispersity index on the clinical applications of lipidic nanocarrier systems. Pharmaceutics. 2018;10(2):57. doi: 10.3390/pharmaceutics10020057.

[44] Barhoum A, García-Betancourt ML, Rahier H, et al. Physicochemical characterization of nanomaterials: polymorph, composition, wettability, and thermal stability. In Emerging applications of nanoparticles and Architecture Nanostructures. Current Prospects of Future Trends. Elsevier; 2018, p. 255–278.

[45] Krishnamurthy S, Esterle A, Sharma NC, et al. Yucca-derived synthesis of gold nanomaterial and their catalytic potential. Nanoscale Res. Lett. 2014;9:1.

[46] Edelmann A, Diewok J, Schuster KC, et al. Rapid method for the discrimination of red wine cultivars based on mid-infrared spectroscopy of phenolic wine extracts. J Agric Food Chem. 2001;49(3):1139–1145. doi: 10.1021/jf001196p.

[47] Fernández K, Agosin E. Quantitative analysis of red wine Tannins using Fourier-transform mid-infrared spectrometry. J Agric Food Chem. 2007;55(18):7294–7300. doi: 10.1021/jf071193d.

[48] Dash SS, Bag BG. Synthesis of gold nanoparticles using renewable Punica granatum juice and study of its catalytic activity. Appl Nanosci. 2014;4(1):55–59. doi: 10.1007/s13204-012-0179-4.

[49] Coates J. Interpretation of infrared spectra, a practical approach. Encycl Anal Chem. 2000;12:10815–10837. doi: 10.1002/9780470027318.a5606.

[50] Balashanmugam P, Balakumaran MD, Murugan R, et al. Phytogenic synthesis of silver nanoparticles, optimization and evaluation of in vitro antifungal activity against human and plant pathogens. Microbiol Res. 2016;192:52–64. doi: 10.1016/j.micres.2016.06.004.

[51] Veeraputhiran V. Bio-catalytic synthesis of silver nanoparticles. 2013;5(5):2555–2562.

[52] Choudhari AS, Mandave PC, Deshpande M, et al. Phytochemicals in cancer treatment: from preclinical studies to clinical practice. Front Pharmacol. 2019;10:1614. doi: 10.3389/fphar.2019.01614.

[53] Pazyar N, Yaghoobi R, Rafiee E, et al. Skin wound healing and phytomedicine: a review. Skin Pharmacol Physiol. 2014;27(6):303–310. doi: 10.1159/000357477.

[54] Sharma A, Khanna S, Kaur G, et al. Medicinal plants and their components for wound healing applications. Futur J Pharm Sci. 2021;7(1):53. doi: 10.1186/s43094-021-00202-w.

[55] Nayak BS, Ramdath DD, Marshall JR, et al. Wound-healing activity of the skin of the common grape (Vitis Vinifera) variant, Cabernet

Sauvignon. Phytother Res. 2010;24(8):1151–1157. doi: 10.1002/ptr.2999.

[56] Afshar M, Hassanzadeh-Taheri M-M, Zardast M, et al. The angiogenetic effect of resveratrol on dermal wound healing in Balb/C mice. Mod. Care J. 2017;14(4). doi: 10.5812/modernc.66118.

[57] Sani A, Cao C, Cui D. Toxicity of gold nanoparticles (AuNPs): a review. Biochem Biophys Rep. 2021;26:100991. doi: 10.1016/j.bbrep.2021.100991.

[58] Mitra I, Mukherjee S, Reddy Venkata PB, et al. Benzimidazole based Pt(II) complexes with better normal cell viability than cisplatin: synthesis, substitution behavior, cytotoxicity, DNA binding and DFT study. RSC Adv. 2016;6(80):76600–76613. doi: 10.1039/C6RA17788C.

[59] Bowler PG, Duerden BI, Armstrong DG. Wound microbiology and associated approaches to wound management. Clin Microbiol Rev. 2001;14(2):244–269. doi: 10.1128/CMR.14.2.244-269.2001.

[60] Lambrechts IA, Thipe VC, Katti KV, et al. Targeting acne bacteria and wound healing in vitro using Plectranthus aliciae, rosmarinic acid, and tetracycline gold nanoparticles. Pharmaceuticals. 2022;15(8):933. doi: 10.3390/ph15080933.

[61] Arciero JC, Mi Q, Branca M, et al. Using a continuum model to predict closure time of gaps in intestinal epithelial cell layers. Wound Repair Regen. 2013;21(2):256–265. doi: 10.1111/j.1524-475X.2012.00865.x.

[62] Dinica RM, Sandu C, Botezatu AVD, et al. Allantoin from valuable Romanian animal and plant sources with promising anti-inflammatory activity as a nutricosmetic ingredient. Sustain. 2021;13(18):10170. doi: 10.3390/su131810170.

[63] Boomi P, Ganesan R, Poorani GP, et al. Phyto-engineered gold nanoparticles (AuNPs) with potential antibacterial, antioxidant, and wound healing activities under in vitro and in vivo conditions. Int J Nanomedicine. 2020;15:7553–7568. doi: 10.2147/IJN.S257499.

[64] Elbagory A, Meyer M, Cupido C, et al. Inhibition of bacteria associated with wound infection by biocompatible green synthesized gold nanoparticles from South African plant extracts. Nanomaterials. 2017;7(12):417. doi: 10.3390/nano7120417.

[65] Pivodová V, Franková J, Galandáková A, et al. In vitro AuNPs' cytotoxicity and their effect on wound healing. Nanobiomedicine. 2015;2:7. doi: 10.5772/61132.